

APPROACHES FOR FINITE ELEMENT SIMULATIONS OF FRP-STRENGTHENED CONCRETE BEAMS AND SLABS

Kenneth W. NEALE ^a, Ahmed GODAT ^b, Hussien M. ABDEL BAKY ^c,
Walid E. ELSAYED ^d and Usama A. EBEAD ^e

^a Adjunct Prof.; Department of Civil Engineering, Université de Sherbrooke, Sherbrooke, Quebec, Canada, J1K 2R1
E-mail address: *Kenneth.Neale@USherbrooke.ca*

^b Dr.; Post-doctoral Fellow; Department of Construction Engineering, École de Technologie Supérieure, Université du Québec, Montreal, Quebec, Canada, H3C 1K3
E-mail address: *Ahmed.Godat@etsmtl.ca*

^c Dr.; Post-doctoral Fellow; Department of Civil and Environmental Engineering, University of Waterloo, Waterloo, Ontario, Canada N2L 3G1
E-mail address: *habdelba@uwaterloo.ca*

^d Dr.; Exp Services Inc., Toronto, Ontario, Canada, M6A 3B6
E-mail address: *Walid.Elsayed@exp.com*

^e Associate Prof.; Civil and Environmental Engineering Department, United Arab Emirates University, Al Ain, UAE
E-mail address: *uebead@uaeu.ac.ae*

Received: 15.09.2011; Revised: 26.10.2011; Accepted: 15.12.2011

Abstract

This paper presents the nonlinear finite element modelling of reinforced concrete members externally strengthened with fibre reinforced polymers (FRPs). Modelling approaches for various applications are reviewed, including the flexural and shear strengthening of beams, as well as the FRP strengthening of two-way slabs. Two types of strengthening methods are considered; namely externally bonded and mechanically fastened FRP strengthening schemes. In all applications, special attention is paid to the implementation of appropriate constitutive models for the FRP/concrete interfaces. To obtain accurate predictions, these models must be capable of properly simulating interfacial stresses and strains, as well as characterizing possible debonding failures. The performance of the various numerical models is assessed through comparisons with appropriate experimental data. It is shown that, with adequate interface models, the numerical predictions can compare very well with experimental measurements in terms of ultimate load carrying capacities, load-deflection relationships and failure modes. The numerical analyses are shown to provide useful insight into phenomena that are difficult to obtain experimentally (e.g., interfacial stress distributions and interfacial slip profiles).

Streszczenie

W artykule przedstawiono sposób modelowania za pomocą nieliniowych elementów skończonych żelbetowych elementów zewnętrznie wzmocnionych polimerami FRP. Omówiono sposoby modelowania dla różnych zastosowań, w tym dla belek wzmocnianych na zginanie i ścinanie, jak również wzmocnienie FRP krzyżowo zbrojonych płyt. Rozważano dwie metody wzmocnienia, a mianowicie zewnętrznie przyspajane oraz mechanicznie przymocowane wzmocnienie FRP. We wszystkich zastosowaniach specjalną uwagę zwracano na zastosowanie odpowiedniego modelu konstytutywnego dla powierzchni styku betonu z FRP. Aby otrzymać dokładne wyniki, modele te muszą mieć możliwość właściwego odwzorowania naprężeń i odkształceń na powierzchni styku, jak również charakteryzować się możliwością zniszczenia przez odspojenie materiału wzmocniającego od podłoża. Wyniki otrzymane z obliczeń numerycznych oceniono poprzez porównanie z odpowiednimi danymi doświadczalnymi. Pokazano, że stosując odpowiednie modele powierzchni styku, wyniki numerycznych obliczeń bardzo dobrze odpowiadają pomiarom doświadczalnym, w zakresie nośności, zależności pomiędzy obciążeniem i ugięciem oraz sposobu zniszczenia. Analizy numeryczne pokazano aby uzyskać przydatny wgląd w zjawiska, które trudno uzyskać doświadczalnie (np. rozkład naprężeń czy charakterystykę poślizgu na powierzchni styku).

Keywords: Finite element analysis; FRP strengthening; Reinforced concrete; Beams; Two-way slabs; Flexure; Shear; FRP/concrete interface.

1. INTRODUCTION

The use of fibre reinforced polymers (FRPs) for the repair and strengthening of existing structures has become a fairly familiar rehabilitation technique. To address this issue, numerous experimental studies have confirmed the effectiveness of externally bonded FRPs to repair and strengthen concrete structures. The performance, however, is compromised when the FRP debonds from the adjacent concrete substrate before the ultimate strength of the FRP has been reached. Clearly, there is a distinct advantage to being able to numerically simulate the complex behaviour of FRP-strengthened members. Nonetheless, experimental results are still required to validate numerical predictions. A survey of the literature shows that most numerical studies on FRP-strengthened members have reported quite satisfactory predictions of the overall behaviour, in particular when the load-deflection curves are examined. However, the results obtained from the existing models are generally not accurate enough to predict the various failure mechanisms. This is particularly true when the adhesive layer is usually not properly taken into account and the simple assumption of full strain compatibility between the concrete and strengthening composites is adopted [1].

As far as numerical studies on FRP-strengthened beams are concerned, researchers have recently attempted to simulate the behaviour of the beams using finite element techniques. The complex behaviour of the strengthened structures has led some researchers to use a linear elastic analysis to address the interfacial behaviour before cracking [2]. A more advanced finite element model, the layer-by-layer numerical technique, was introduced to take into consideration the material nonlinearities of the concrete before and after cracking, and also to include the effect of tension stiffening [3-5]. These analytical models were proposed to predict the load deflection behaviour and the ultimate load carrying capacities; however, they did not simulate the debonding failure modes or specifically address the interfacial behaviour. The assumption of full strain compatibility between the concrete and the FRPs is not realistic and leads to overestimated predictions in terms of FRP strains and member stiffnesses. Therefore, an appropriate model that can describe the FRP/concrete interfacial behaviour is essential.

When debonding failures occur, they usually result from a shear failure of a thin layer of concrete adjacent to the adhesive. Adhesives currently used in FRP strengthening applications generally ensure that

the bond strength of the adhesive is sufficient to transfer the interfacial stresses from the FRP to the concrete or vice versa. As a result, researchers have concluded that the bond strength of an externally bonded FRP depends mainly on the quality of the surface preparation and the quality of the concrete itself, especially its shear strength. In finite element analyses, two approaches have been adopted to simulate the debonding. In the first approach, debonding is simulated by modelling the cracking and failure of the concrete elements adjacent to the adhesive layer. This approach, which is referred to as the meso-scale model, uses a very fine mesh with element sizes (0.2-0.5 mm) being one order smaller than the thickness of the fracture layer of the concrete [6]. The advantage of this approach is that it models the thin concrete layer adhering to the FRP where the debonding occurs. However, it generally requires large computational resources. In the second approach, interface elements are used to predict the nonlinear behaviour between the FRP and concrete [7]. In the present study a combination of the two approaches is used. The bond stress-slip model developed by Lu et al. [6] based on the meso-scale model is implemented to simulate the FRP/concrete interfacial behaviour via interface elements. It is thought that this can lead to accurate FRP/concrete interfacial responses, while minimizing computational demands.

In this paper, we review some of the finite element models developed by the authors to simulate the behaviour of FRP flexurally-strengthened beams [8, 9], FRP shear-strengthened beams [10, 11] and FRP-strengthened two-way slabs [12, 13]. The key feature of these models is the inclusion of interface elements that are able to properly represent the FRP/concrete interfacial behaviour. For FRP-strengthened two-way slabs, both the conventional FRP external bonding method as well as the mechanically fastened FRP technique are considered. The accuracy of the numerical models is evaluated by comparing the numerical predictions to previously reported experimental results. Once the accuracy of the models is established, the numerical models are then exploited to investigate complex mechanisms that are difficult to characterize experimentally, such as interfacial stress distributions, interfacial slip profiles, and shear crack angles.

2. FINITE ELEMENT MODEL

In this study, a three-dimensional finite model is developed to simulate the behaviour of FRP-strengthened members. The initial phase of the numerical study involves the development of accurate finite element models for the reference (unstrengthened) specimens. The quality of the model is assessed by comparing the numerical results with experimental measurements. In the second phase of the numerical study, the reference specimens are modified to include the presence of external FRPs for strengthening. The accuracy of the model is also measured through comparisons with experimental data. The goal of these phases was to insure that the numerical models accurately represent the actual tested specimens. All computations were performed using the ADINA finite element software [14]. The features of the numerical model are detailed below.

Material Modelling

Concrete

Various constitutive models have been adopted in simulations of externally-strengthened beams and slabs to describe the behaviour of concrete under a wide range of complex stress and strain histories. These models included nonlinear elastic models, plasticity-based models whether perfect plasticity models, or elastic-plastic models. In general, the existing non-linear elasticity or plasticity-based concrete models have been relatively successful in predicting the load-deflection behaviour of FRP-strengthened beams and slabs. This is because of the fact that the behaviour depends mainly on the tensile and cracking behaviour of the concrete, while the compressive behaviour plays a secondary role.

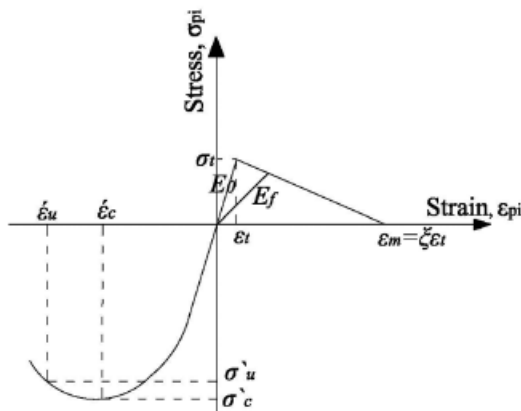


Figure 1. Typical uniaxial stress-strain curve for concrete [15]

The constitutive model used for the concrete behaviour is provided in the ADINA software [15]. Figure 1 shows a typical uniaxial stress-strain curve for concrete. It is characterized by a non-linear stress-strain relationship to allow for the strain softening behaviour under increasing compressive stresses. In addition, it utilizes failure envelopes to define failure in either tension, or compression by crushing. It also features a mechanism to model the post-cracking and post-crushing behaviour of the concrete. The failure envelopes also account for multiaxial stress conditions. The tensile behaviour of the concrete takes into account cracking, shear modulus degradation, fracture energy and tension stiffening. Tension stiffening is modelled as a linearly descending branch in the stress-strain relationship after the peak point at which concrete has cracked. Another feature of the concrete model is the fixed crack approach, in which the plane of failure occurs perpendicular to the corresponding principal stress direction. For the finite element implementation, the values of the compressive strength f'_c (MPa), tensile strength f_t (MPa) and elastic modulus E_c (MPa) are taken from the corresponding experimental set of data. When f_t and E_c are not given, they are approximated based on the following CSA [16] equations:

$$f_t = 0.6\sqrt{f'_c} \text{ (MPa)} \quad (1)$$

$$E = 3300\sqrt{f'_c} + 6900 \text{ (MPa)} \quad (2)$$

A hypoelastic (incremental) model is used to describe the nonlinear stress-strain relationship of the concrete. It is assumed that the strain increment vector $\{\epsilon\}$ is linearly related to the stress increment vector $\{\sigma\}$ through the material response moduli $[C]$, which can be written in a matrix form as:

$$\{\sigma\} = [C]\{\epsilon\} \quad (3)$$

The matrix of tangential moduli $[C]$ assumes an orthotropic material with the directions of orthotropy being defined by the principal stress directions. It has the following form:

$$C = 1/(1+2\nu) \times \begin{pmatrix} E_{p1} & \nu E_{12} & \nu E_{13} & 0 & 0 & 0 \\ E_{p2} & \nu E_{23} & 0 & 0 & 0 & 0 \\ E_{p3} & 0 & 0 & 0 & 0 & 0 \\ 0.5(1-2\nu)E_{12}/(1+\nu) & 0 & 0 & 0 & 0 & 0 \\ \text{Symmetric} & 0.5(1-2\nu)E_{13}/(1+\nu) & 0 & 0 & 0 & 0 \\ & & & & & 0.5(1-2\nu)E_{23}/(1+\nu) \end{pmatrix} \quad (4)$$

where E_{p1} , E_{p2} and E_{p3} are the equivalent multi-axial Young's moduli in the principal directions computed according to the value of the principal strain (ε_{pi}); ν is Poisson's ratio. The equivalent multi-axial Young's moduli required to compute the off-diagonal components of the material response matrix, C , are computed as:

$$E_{ij} = (|\sigma_{pi}|E_{pi} + |\sigma_{pj}|E_{pj}) / (|\sigma_{pi}| + |\sigma_{pj}|) \quad (5)$$

where σ_{pi} is the principal stress value. When the principal stress state lies on the failure envelope, it is assumed that the material strain softens isotropically in all directions, which corresponds to the case of $\varepsilon_{pi} \leq \varepsilon_u$ (ε_u and σ_u are the concrete ultimate tensile strain and tensile stress, respectively). The stresses in the principal directions are assumed to linearly reduce to zero using the following modulus:

$$E_{pi} = (\sigma_u - \sigma_c) / (\varepsilon_u - \varepsilon_c) \quad (6)$$

To identify whether the material has failed or cracked, the principal stresses are used to locate the current stress state. Having established the principal stress σ_{pi} with $\sigma_{p1} \geq \sigma_{p2} \geq \sigma_{p3}$, the stresses σ_{p1} and σ_{p2} are held constant and the minimum stress value that would have to be reached in the third direction to cause crushing is calculated using the failure envelopes. If the stress state corresponding to σ_{p2} and σ_{p3} lies on or outside the biaxial failure envelope, then material failure has occurred. For the tensile failure envelope, it is assumed that the tensile strength of the concrete in a principal direction does not depend on the tensile stresses in other principal stress directions.

The concrete is assumed to behave as an isotropic linear material for tensile stresses less than the tensile strength value. When the principal tensile stress exceeds its limiting value, a crack is assumed to occur in a plane normal to the direction of the corresponding principal strain, and this crack direction is then fixed for subsequent loading (fixed smeared crack model). The effect of the concrete cracking is that the normal and shear stiffness, E_c and G_c , respectively, across the plane of cracks are reduced using reduction factors η_n and η_s , respectively. The factors η_n and η_s imply a sudden drop of the initial stiffness E_c in the direction of the crack and the shear stiffness G_c in the plane of tensile cracks, respectively. When the principal tensile strain, $\varepsilon_t \leq \varepsilon \leq \varepsilon_m$, the secant Young's modulus E_t replaces the norm $E_c \eta_n$ in the material

response matrix (where ε_m is the concrete maximum tensile strain). Beyond the strain level, ε_m , the factor η_n is taken 0.0001 to avoid the possibility of a singular stiffness matrix. The factor η_s , known as the shear reduction factor, is assumed 1.0 before cracking. Then η_s is reduced linearly to be 0.5 at the maximum tensile strain level (ε_m) and remains constant to consider several physical factors such as aggregate interlock, reinforcement dowel action and friction between cracks. The amount of tension stiffening (ξ) computed at each integration point is as follows:

$$\xi = \frac{2E_c G_f}{f_t^2 h} \quad (7)$$

where h is the width of the finite element perpendicular to the plane of tensile cracks and G_f is the concrete fracture energy released per unit area. If the normal strain across the existing crack becomes greater than that just before crack formation, the crack is assumed to open; otherwise, it is closed.

Steel Reinforcement and FRP Composites

The steel reinforcement is represented by an elastic-plastic constitutive relation with linear strain hardening. The ratio between the slopes in the elastic range to those in the plastic range is taken as 100. To indirectly include the effect of the dowel action, an increased value for the shear retention factor is used. A linear elastic tensile model until failure is assumed to represent the FRP composites. A rupture point on the stress-strain relationship defines the maximum stress and strain of the FRP composites.

FRP/Concrete Interface

The bond stress-slip models developed by Lu et al. [6] have received wide acceptance and are considered to be accurate models that can be incorporated into a finite element analysis. The behaviour of the FRP/concrete interface is simulated by a relationship between the local shear stress, τ , and relative displacement, s . Three different bond stress-slip relations have been suggested by these authors; they are classified according to their level of sophistication and are respectively referred to as the "precise", the "simplified" and the "bilinear" models. It should be noted that the interfacial fracture energy values calculated with the three models are essentially identical. The interfacial fracture energy is the area under the τ - s curve, which corresponds to the energy per unit bond area required for complete debonding of

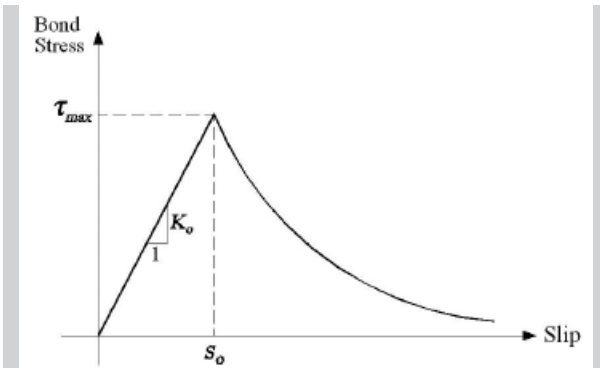


Figure 2. Bond-slip model for beams and two-way slabs strengthened with conventional technique [6]

the laminate. These bond stress-slip models are explained in detail in Lu et al. [6]. The model is shown in Fig. 2 and formulated as follows:

Considering τ_{max} to be the maximum bond stress and s_0 the corresponding slip, then for the ascending part; i.e., $s < s_0$

$$\tau = \tau_{max} \frac{s}{s_0} \tag{8}$$

The value of τ_{max} is related to the tensile strength of the concrete, f_t , according to the following equation:

$$\tau_{max} = 1.5\beta_w f_t \tag{9}$$

The value of s_0 is also related to f_t according to the following equation:

$$s_0 = 0.0195\beta_w f_t + s_e \tag{10}$$

The factor β_w refers to the FRP width factor. It is related to the ratio between the width of the FRP, b_f , and that of the concrete structural element, b_c , and is calculated from the following equation:

$$\beta_w = ((2.25 - b_f / b_c) / (1.25 + b_f / b_c))^{0.5} \tag{11}$$

In Equation (10)

$$s_e = \tau_{max} / K_0 \tag{12}$$

The value of K_0 is given by

$$K_0 = K_a K_c / (K_a + K_c) \tag{13}$$

where

$$K_a = G_a / t_a \tag{14}$$

$$K_c = G_c / t_c \tag{15}$$

Here G_a and t_a , and G_c and t_c are the shear modulus and the thickness of the adhesive and concrete, respectively. The value of t_c is taken as 5 mm; this corresponds to the effective thickness whose deformation forms part of the interfacial slip [6].

For the descending part, i.e., $s > s_0$

$$\tau = \tau_{max} \exp[-\alpha(s / s_0 - 1)] \tag{16}$$

where

$$\alpha = \frac{1}{\frac{G_f}{\tau_{max} s_0} - \frac{2}{3}} \tag{17}$$

The interfacial energy G_f is calculated according to the following equation:

$$G_f = 0.308 \beta_w^2 \sqrt{f_t} f(K_a) \tag{18}$$

In the original model by Lu et al. [6], the function $f(K_a)$ was set equal to 1 for normal adhesives.

For mechanically fastened FRP-strengthened two-way slabs, bearing stress-slip models developed by Elsayed et al. [17] are employed to address the mechanically fastened FRP/concrete interfacial behaviour. These models are established based on the average experimental results of one fastener FRP/concrete connection. Both shot and threaded fasteners were considered in this study. Regression analysis was used to obtain a good agreement between the analytical models and the experimental data. The FRP/concrete mechanical behaviour was modelled as a relationship between the local bearing stress and the relative displacement s between the FRP strip and the concrete. The σ - s relationships, as shown in Fig. 3, are proposed as follows:

$$\sigma = \frac{\sigma_b s}{s_b} \quad \text{if } s \leq s_b \tag{19}$$

$$\sigma = \sigma_b A^{\exp(-\alpha A^{\beta})} \quad \text{if } s_b < s < s_f \tag{20}$$

$$\sigma = \frac{\sigma_b}{0.167 \cosh B^{2\beta}} - \frac{\sigma_f}{0.496 \sinh B^{2\beta}} \quad \text{if } s \geq s_f \tag{21}$$

(for short fasteners)

$$\sigma = \sigma_f \quad \text{if } s \geq s_f \text{ (for screwed fasteners)} \tag{22}$$

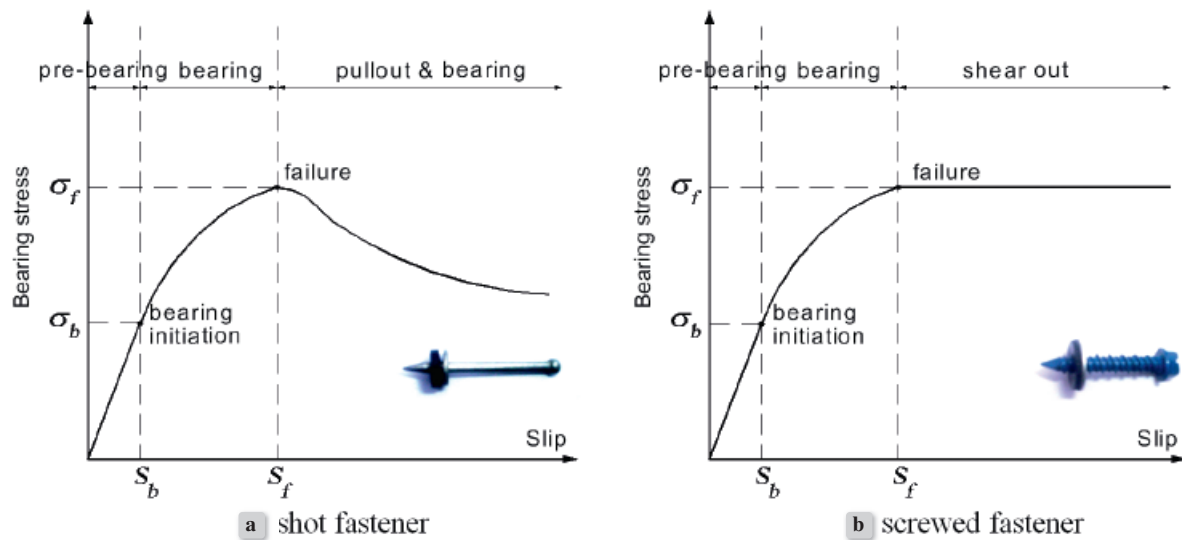


Figure 3. Bearing-slip models for two-way slabs strengthened with mechanical fastening [17]

where

$$A = s/s_b, B = s/s_f \quad (23)$$

In these expressions, σ_b is the bearing yield stress of the FRP strip, which is taken to be 234 MPa as provided by the manufacturer, and s_b is the corresponding slip, determined experimentally to be 2 mm. The variable σ_f is the bearing strength of the FRP strips and s_f is the corresponding slip, as shown in Figs. 3(a) and (b). The value of σ_b is equal to 335 MPa and to 385 MPa for the shot and screwed fasteners, respectively. According to the experimental observations, s_f was taken to be 9 mm. The factors α and β were equal to 0.868 and 0.333 for the shot fasteners and to 0.521 and 0.50 for the screwed fasteners, respectively. These factors were determined so that a best-fit could be obtained between the models and the experimental curves obtained for a single fastener. Numerical implementations were conducted to validate these bearing-slip models by considering the MF-FRP/concrete joints having multiple fasteners.

Structural Modelling

Concrete, Steel Reinforcement and FRP Composites

Three-dimensional brick elements with three degrees of freedom per node are employed to model the concrete. Using such elements satisfies shear and bending deformations due to their quadratic interpolation functions. The steel reinforcement embedded in the concrete is represented by truss elements. Ideally, the

bond strength between the concrete and steel reinforcement should be considered. However, in the current application, the truss elements representing the longitudinal steel and steel stirrups are directly connected to the concrete elements. Debonding that may occur between the steel reinforcement and the surrounding concrete is accounted for in the tension stiffening model of the concrete. This is carried out by increasing the value of the tension stiffening branch up to specific limit for the reference specimen. The value of the tension stiffening is taken constant for the strengthened specimen.

A study was carried out by Godat et al. [18] to compare two alternate elements to represent the behaviour of the FRP composites; namely, truss elements and shell elements. They found that shell elements are more appropriate when their orthotropic nature is accounted for in the constitutive relation for the material.

FRP/Concrete Interface

To represent the bond stress-slip between the concrete and FRP composites, bilinear truss elements aligned in a discrete manner are employed. These elements allow relative movements between the two adjacent surfaces, as shown in Fig. 4(a). The interface elements are arranged parallel to the fibre orientation and full strain compatibility is assumed in the other direction. It is necessary to emphasize that these interface elements do not directly represent the adhesive. They represent the overall FRP/concrete

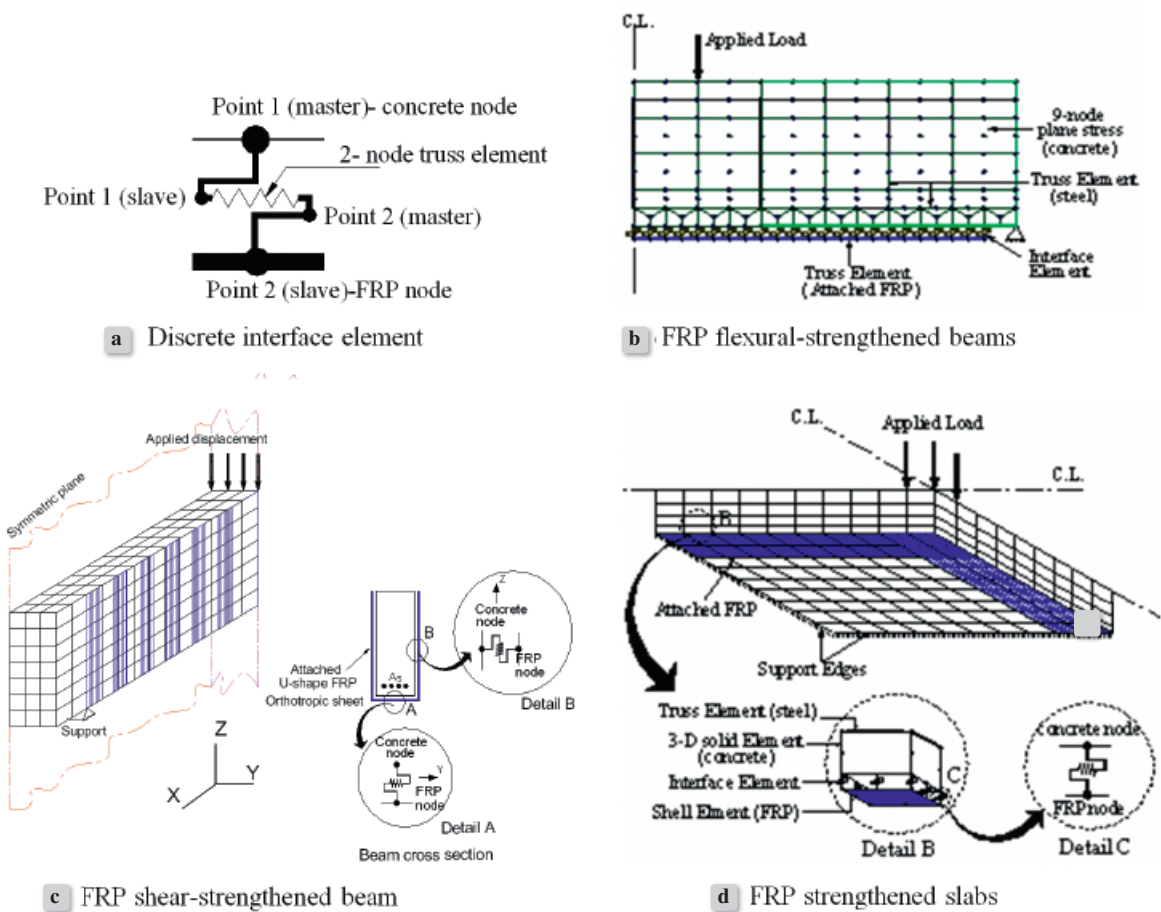


Figure 4.
Finite element models

interfacial response, which depends on the concrete, the FRP and the adhesive. As shown in Fig. 4(a), each interface element connects the FRP nodes and the corresponding concrete nodes; the interface elements are totally independent from each other. The total displacement between so called “slave” (Point 1) and “master” (Point 2) nodes of the interface element represents the interfacial slip. The discontinuities of the discrete truss elements allow each interface element to fluctuate from negative to positive stresses depending on their distance from the crack. The constitutive law of these elements (τ - ϵ) depends on their length. The difference in the displacement between the concrete and FRP represents the slip at the interface, while the axial stress in these elements indicates the interfacial stress. For the mechanically fastened FRP-strengthened two-way slabs, an interface element is used at each fastener location. Typical geometrical representations and the types of elements used for the FRP flexure-strengthened beams, the FRP shear-strengthened beams and

FRP-strengthened two-way slabs are shown in Figs. 4(b), (c) and (d), respectively.

Specimens Investigated

The validity of the numerical model is investigated using published experimental data having different FRP strengthening configurations and material properties. These are selected for the numerical analysis so as to cover the widest possible range of FRP strengthening schemes. For the FRP flexurally-strengthened beams, the finite element models considered the investigation of the FRP debonding at either the plate end or at intermediate cracks. For the FRP shear-strengthened beams, the study included vertical and inclined FRP composites attached to the sides of beams or with U-shaped wraps for rectangular and T-sections. With regard to slab strengthening, various FRP configurations were considered with both passive as well as pre-stressed FRP strengthening with either the conventional bonding method or the mechanical fastening

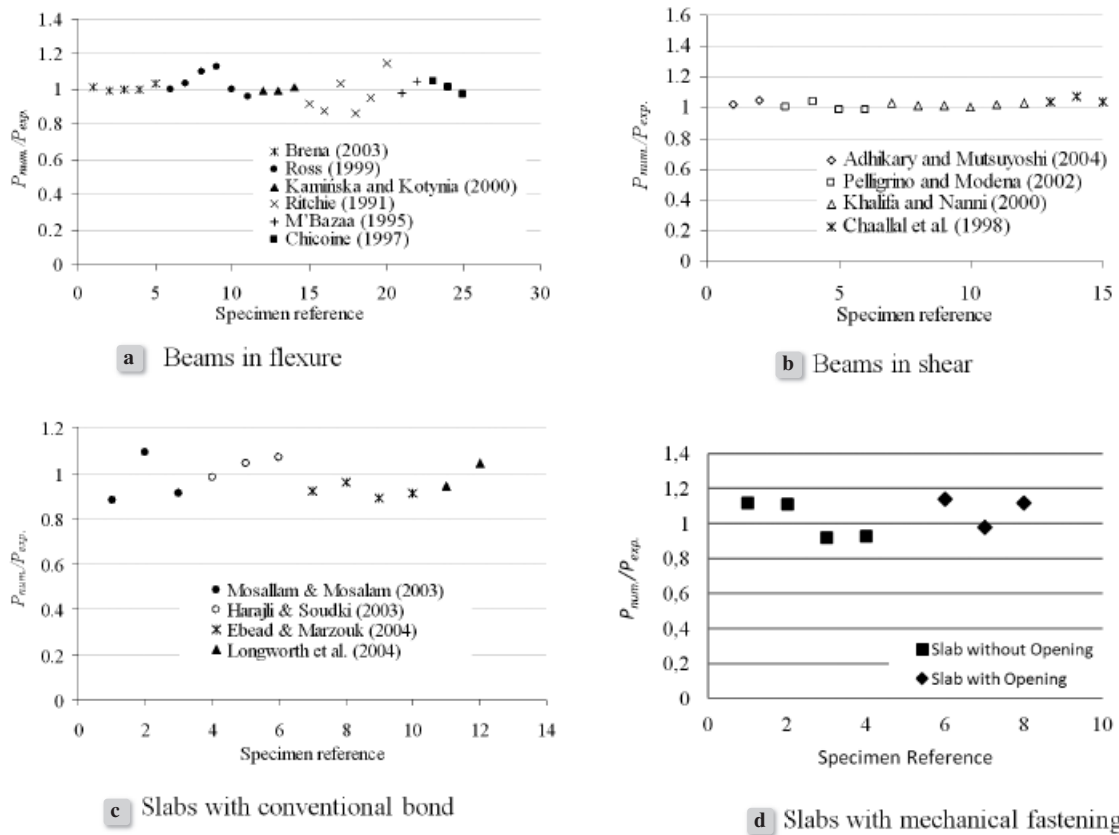


Figure 5. Comparison between experimental-to-numerical load carrying capacities

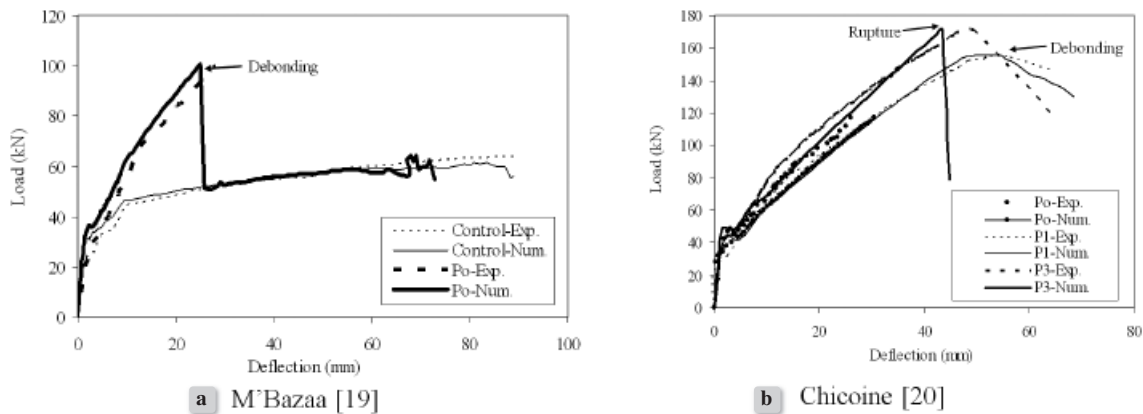


Figure 6. Load-deflection relationships for FRP flexural-strengthened beams

method for FRP composites. As well, the finite element model included two-way slabs without openings and others comprising an opening at the centre of the slabs. The nonlinear load-deformation behaviour of the structure was simulated under displacement-controlled loading conditions. In view of the geometrical

and loading symmetries, only one quarter of the specimens were simulated.

3. NUMERICAL RESULTS AND DISCUSSION

The results presented in the subsequent sections are in terms of ultimate load carrying capacities, load-deflection relationships and failure modes for the different applications simulated in this study. Special concerns are placed on the results for the interfacial behaviour between the FRP laminates and the concrete in terms of the interfacial stress distributions and slip profiles. The specimen notations here correspond to those employed in the original references.

Ultimate load carrying capacities

Figures 5(a) and 5(b) depict the numerical-to-experimental ratios of the load capacities for the beams strengthened in flexure and in shear, respectively. The experimental results of 25 flexurally-strengthened beams are used to assess the validity of the finite element model [8]. In addition, 15 shear-strengthened beams are considered [10]. As can be seen in these figures, there is a very good agreement between the numerical predictions of the ultimate load capacities and the experimental data. The ultimate capacity of a beam represents the load at which the concrete is crushed in compression, or at which the FRP has debonded or ruptured. The average numerical-to-experimental load capacity ratio for the FRP flexurally-strengthened beam applications is 100.3% with a standard deviation of 6.5%. As shown in Fig. 5(b), the corresponding values of the average and the standard deviation in case of the FRP shear-strengthened beams are 102% and 2.31%, respectively, thus indicating an excellent agreement.

With regard to the two-way slabs strengthened with the conventional external FRP bonding method (Fig. 5c), a very good agreement is obtained when comparing the numerical results with the experimental data of 12 different specimens with an average numerical-to-experimental load capacity ratio of 97% with a standard deviation of 7.3% [12]. For the FRP mechanically fastened two-way slabs (Fig. 5d), reasonable accuracy is obtained between the numerical predictions and the experimental results [13]. The average accuracy (numerical-to-experimental) and corresponding standard deviation are 1.043 and 0.1, respectively.

Load-deflection relationships and failure modes

The numerical results shown in Fig. 6 are for the numerical versus experimental comparisons in terms

of the load-deflection relationships for selected beam specimens [19, 20]. Debonding of the FRP laminates off the concrete surface caused most of the failures that were observed experimentally. As can be seen from Fig. 6(a) for the strengthened Specimen P0 tested by M'Bazaa [19], we were able to not only capture the debonding load, but also the complete post-debonding plateau until complete failure. Generally speaking, experimental post-failure measurements of the loads and the associated deflections are quite difficult and generally not very accurate. This explains the discrepancy in the post-failure region for Specimen P1 in the work of Chicione [20] (Fig. 6b), for example, in which the failure occurred due to the rupture of the FRP (the failure mode actually predicted in our analysis). We can conclude that the proposed models are able to simulate the entire load-deflection relationships, including the descending and post failure profiles, in view of the displacement-controlled solution adopted in these analyses.

Figures 7(a) and 7(b) present the numerical/experimental comparisons of the load deflection relationships for the shear-strengthened specimens tested by Pellegrino and Modena [21] and Adhikary and Mutsuyoshi [22], respectively. The specimens tested by Pellegrino and Modena used spaced side-bonded FRP laminates, whereas the specimens tested by Adhikary and Mutsuyoshi were strengthened with U-shaped FRP laminates. An excellent agreement is observed between our predictions and the experimental results. The dominant failure mode in these analyses is the delamination of the FRPs as the bond interface failed in shear. This is what was observed experimentally.

The comparisons are depicted in Fig. 8(a) for conventionally strengthened slabs and in Figure 8(b) for mechanically fastened strengthened two-way slabs. With regard to the slabs conventionally strengthened, the comparisons are depicted in Fig. 8(a) for the specimens B2-SL1 (reference specimen) and B2-SL4 (using prestressed FRP laminates) tested by Longworth et al. [23]. The numerical model is successfully simulated the case of prestressed FRP laminates for specimen B2-SL4, and are able to predict the post peak behaviour for all the specimens. Results of the numerical modelling of mechanically fastened two-way slabs without openings tested by Elsayed et al. [12] are shown in Fig. 8(b). As seen in the figure, an excellent agreement is obtained between our predictions and the experimental data.

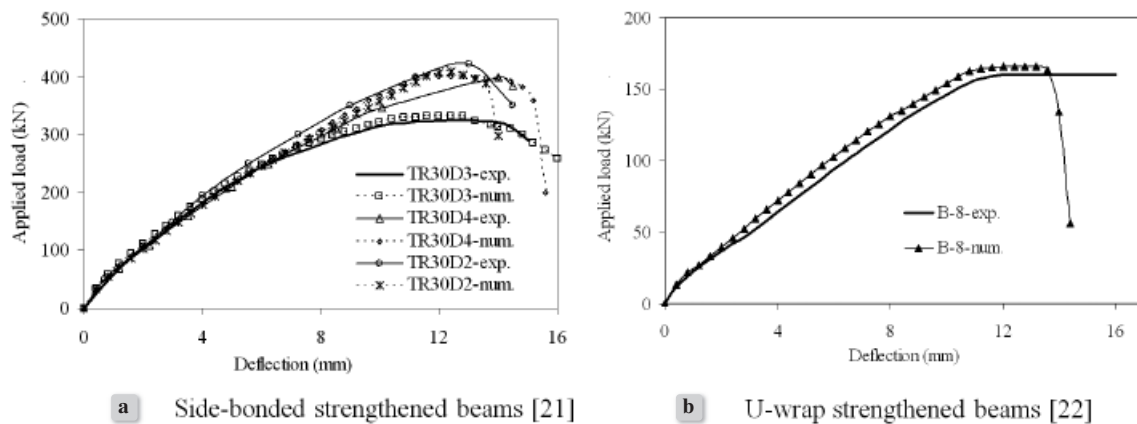


Figure 7. Load-deflection relationships for FRP shear-strengthened beams

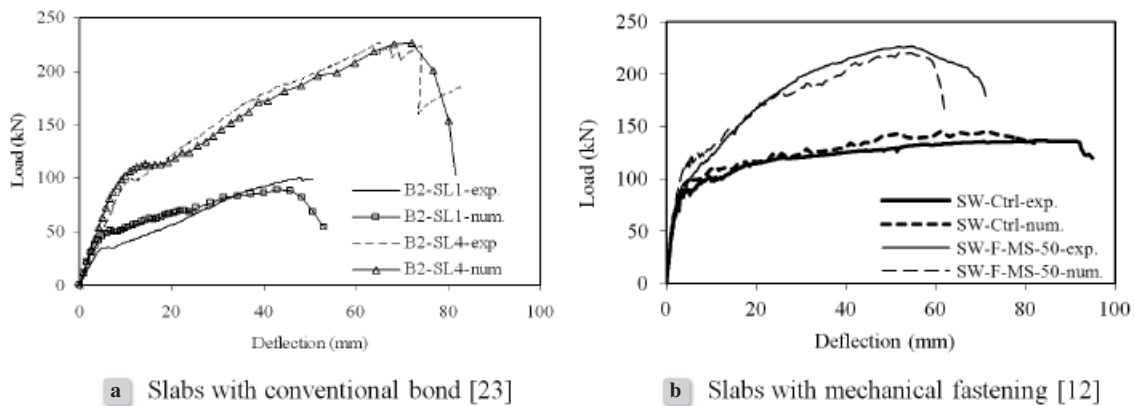


Figure 8. Load-deflection relationships for FRP two-way strengthened-slabs

Interfacial stress distributions

A distinct advantage of having reliable numerical tools is that they can provide valuable insight into phenomena that are very difficult to assess experimentally. For example, knowing the values of the interfacial stresses and slips between the bonded FRPs and concrete can be very helpful for a better understanding of the FRP/concrete interfacial behaviour and bond performance. Interfacial shear stresses play an important role in the performance of bonded FRP laminates. The numerical results presented here are for FRP flexurally-strengthened beams tested by Brena et al. [24]. They illustrate the interfacial behaviour before and after cracking.

Flexural-strengthened beams before cracking

In Fig. 9(a), the shear stress distribution along the FRP/concrete interface before cracking is presented.

At stress levels that are less than the cracking stress, the interfacial shear stress concentration occurs at the plate end and descends to a constant value within a short length ranging from 1.5 to 2.5% of the laminate length measured from the beam centre-line. With an increase of the applied stress up to the cracking stress, the interfacial shear stress linearly increases with a maximum value occurring at the plate end. The interfacial shear stress distribution before cracking is similar to that observed for the direct shear tests, where the maximum shear stress occurs at the plate cut-off point.

Flexurally-strengthened beams after cracking

Crack initiation and propagation mainly controls the interfacial behaviour, while the crack width causes an abrupt slip at the interface. Hence, the slip value is controlled by several factors; namely, the crack width,

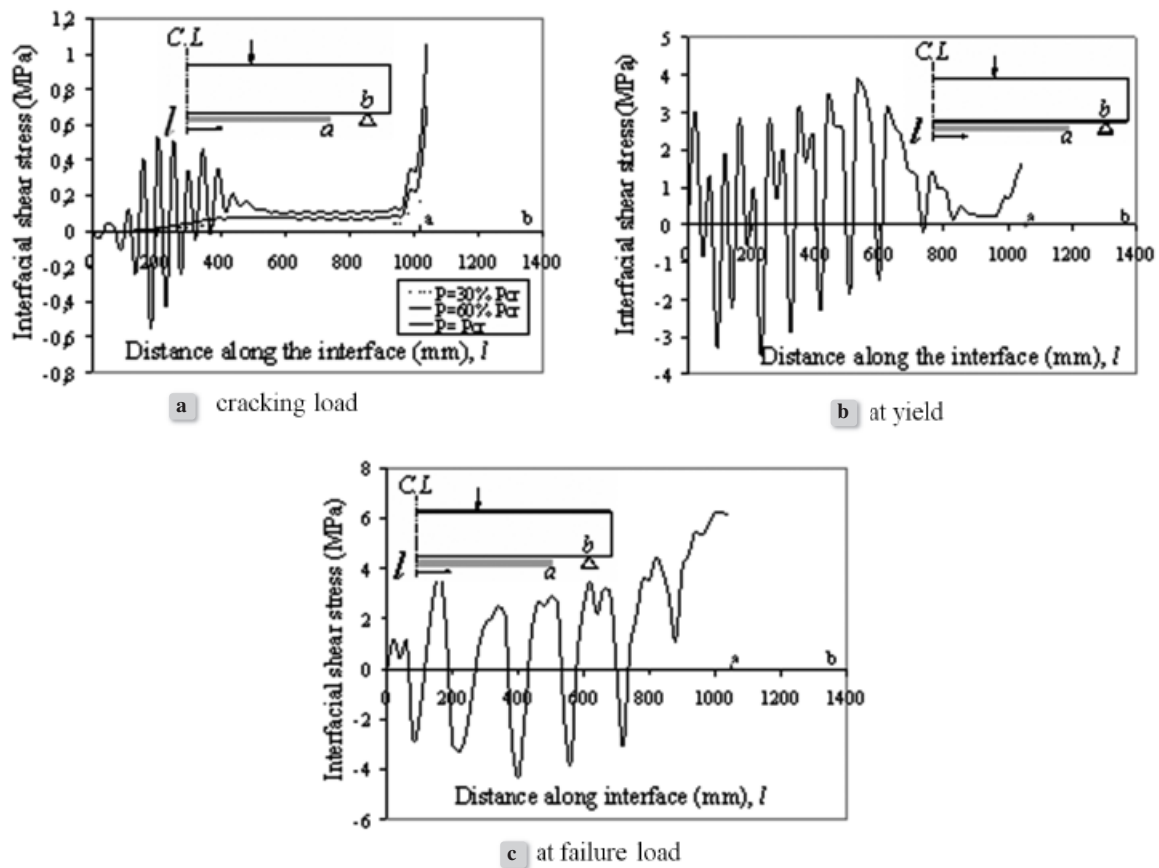


Figure 9. Interfacial shear stress distributions for Specimen A3 [24]

spacing, and number of cracks. At a crack, the interfacial shear stress fluctuates from negative to positive values, as can be seen in Figs. 9(b) and 9(c). With an increase of the applied load up to the yield load, the flexural cracks tend to open; therefore, the maximum bond stress shifts from the plate-end to the mid-span where the flexural cracks have propagated (Fig. 9b). At the failure load and close to it, the flexural cracks become wider and the shear cracks occur near the plate end. As a result, the shear stress dramatically increases in the regions of the flexural cracks near the concentrated load and at the vicinity of the shear cracks close to the plate end, thus causing an end-plate debonding (Fig. 9c).

Interfacial slip profiles

In the following discussions, the capability of the numerical models to capture FRP/concrete interfacial slip profiles for the FRP shear-strengthened beams and FRP-strengthened two-way slabs is presented.

The slip profiles along the sheet depth for FRP shear-strengthened beams are shown in Fig.10(a)-10(c) for specimen TR30D3 tested by Pellegrino and Modena [21]. The figure ((a) to (c)) describes the slip values at three locations corresponding to 150 mm, 400 mm and 600 mm from the point of applied load, respectively. The shear span of the beam considered is 750 mm. On each figure, the slip values are obtained at various load levels up to failure. The presence of a shear crack may be identified by the fluctuating from negative to positive values in the slip profiles. The slip profiles are seen to significantly increase at the vicinity of a shear crack. Furthermore, the locations of the maximum slip values correspond to the shear crack intersections with the FRP composites. For the slip profiles drawn at a distance of 150 mm from the load point (Fig. 10a), the maximum slip value is obtained near the top end of the sheet. For the slip profiles at a distance of 400 mm from the load point (Fig. 10b), the maximum slip value occurs around the mid-depth of the beam. This is attributed

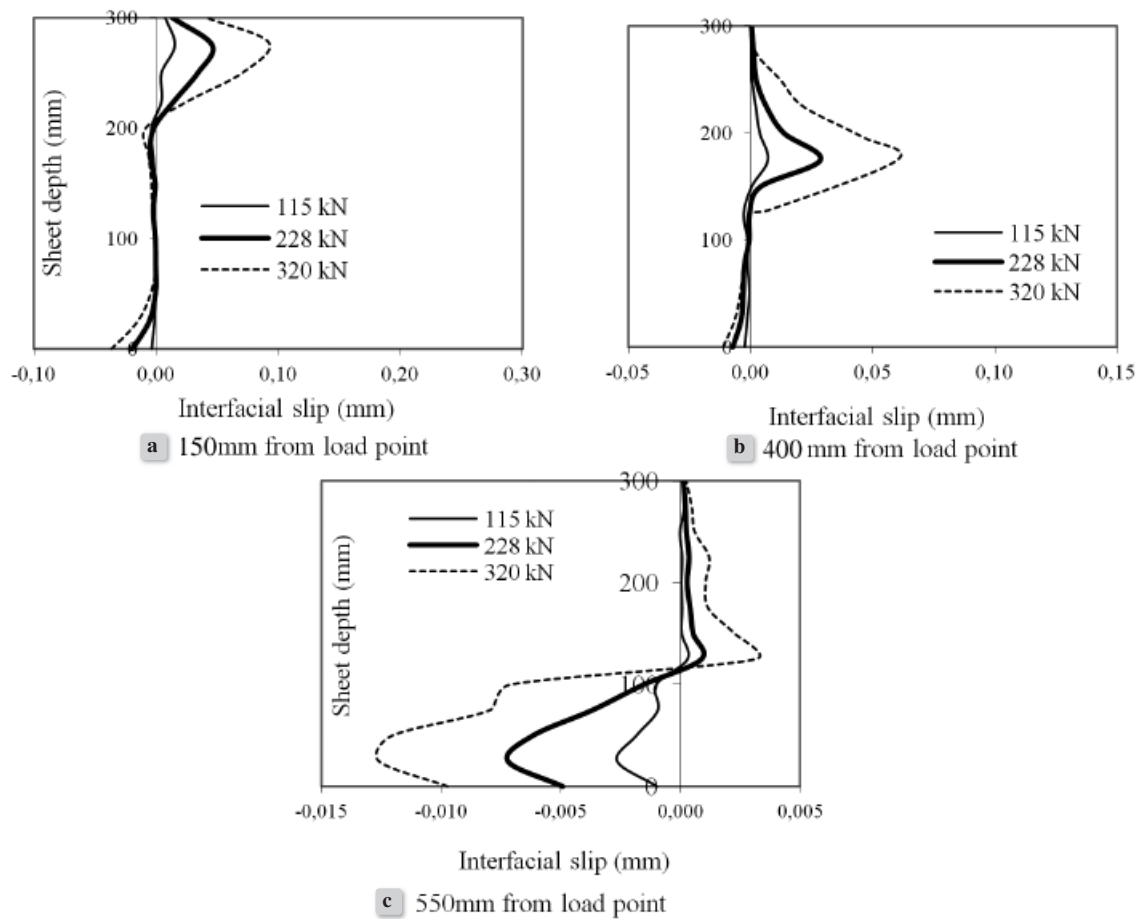


Figure 10. Interfacial slip profiles along the FRP sheet depth for specimen TR30D3 [21]

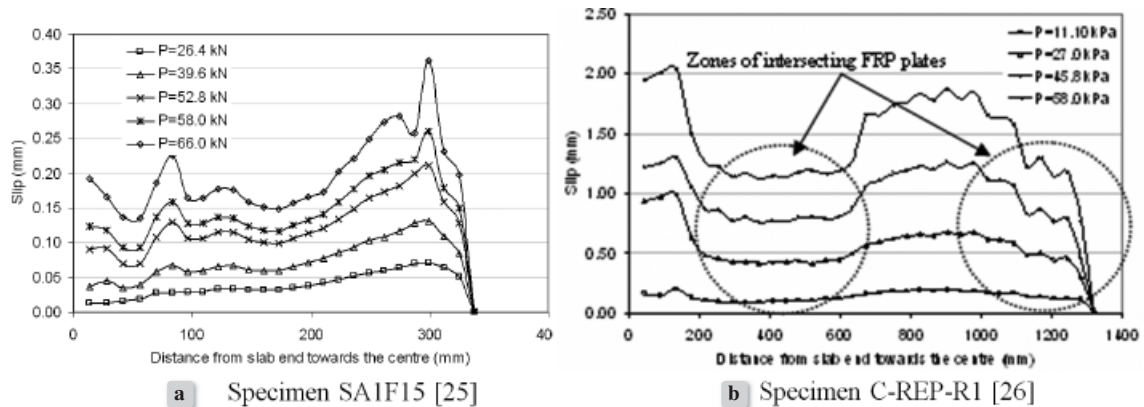


Figure 11. FRP/concrete interfacial slip profiles for two-way slabs

to a local effect caused by a shear crack. For the slip profiles at a distance 600 mm from the load point (Fig. 10c), the slip attains its maximum near the bottom end of the sheet. Generally, shear cracks are

expected to propagate as the load increases and the failure occurs due to debonding of the FRP sheets over the main diagonal shear crack. When using interface elements, the failure mode progress was

very similar to that observed experimentally. Thus, the numerical model is capable to capture the failure process observed experimentally.

Typical predicted FRP/concrete slip profiles, at different load levels, are shown in Fig. 11 for two strengthened two-way slab specimens having different failure modes. Fig. 11(a) shows the predicted slip profiles along the FRP/concrete interfaces for the specimen SA1F15 tested by Harajli and Soudki [25]. It is observed that the slip values at the centre of the slab are significantly higher than those at the end of the laminate. This suggests a punching shear failure associated with debonding of the FRP material in the central region of the slab. In the predicted slip profiles for specimen C-REF-R1 tested by Mosallam and Mosalam [26], we observe zones where the slips are diminished relative to those in the adjacent regions (Fig. 11b). These, in fact, correspond to the areas where the FRP laminates overlap, and where we would indeed expect reductions in the interfacial shear stresses and slips. This result suggests that, in general, the addition of transverse anchorage strips at the ends of the FRP laminates should be quite effective to mitigate debonding failures in these regions.

Shear crack angles

The shear crack angle is a key parameter in the calculation of the FRP shear capacity. The interfacial slip profiles are used to predict the crack formation angle along the shear span for FRP shear-strengthened beams [27]. It can generally be stated that, in the experimental tests, shear cracks propagated as the load increased and failure occurred due to debonding of the FRP over the main diagonal shear crack. The interfacial slip profiles can successfully be utilized to predict the crack formation angle along the shear span. For example, the maximum slip value for the FRP sheet close to the applied load is at the top edge of the FRP sheet (Fig. 10a), whereas the highest slip value for the FRP sheet near the support is at the bottom edge of the FRP sheet (Fig. 10c). The connection of these slip value points can be considered as the track of the crack inclination angle. Results show that the average angle of the maximum slip values, which represents the crack angle, is 26° . They also demonstrate the capability of the model to predict the shear crack angle along the shear span.

4. CONCLUSION

Finite element analyses have been carried out to address the interfacial behaviour of FRP-strengthened reinforced concrete structures. A nonlinear constitutive model was incorporated to represent the interfacial behaviour between the bonded/fastened FRP laminates and concrete substrate. In order to investigate the validity of the numerical models, theoretical predictions have been calibrated against published experimental data. The comparisons between the numerical and experimental results showed very good correlations in terms of the ultimate carrying capacities and load-deflection relationships. Our studies have clearly shown the importance of appropriately modelling the FRP/concrete interface if accurate predictions of the behaviour of externally FRP-strengthened members are to be obtained. This study has also demonstrated that reliable numerical models represent very valuable tools for gaining insight into phenomena that are extremely difficult to assess experimentally.

ACKNOWLEDGEMENTS

This research was funded by the Natural Sciences and Engineering Research Council of Canada (NSERC), the Canadian Network of Centres of Excellence on Intelligent Sensing for Innovative Structures (ISIS Canada) and the Fonds Québécois de la recherche sur la nature et les technologies (FQRNT).

REFERENCES

- [1] Neale K.W., Ebead U.A., Abdel Baky H.M., Elsayed W.E., Godat A.; Analysis of the load-deformation behaviour and debonding for FRP-strengthened concrete structures, *Advances in Structural Engineering*, Vol.9, No.6, 2006; p.751-763
- [2] Ehsani M.R., Saadatmanesh H.; Fibre composite plates for strengthening bridge beams, *Composite Structures*, Vol.15, 1990; p.343-355
- [3] Takahashi Y., Sato Y., Ueda T., Maeda T., Kobayashi A.; Flexural behaviour of RC beams with externally bonded carbon fibre sheet, *Non-Metallic (FRP) Reinforcement for Concrete Structures*, Japan Concrete Institute, Vol.1, 1997; p.327-334
- [4] Nitereka C., Neale K.W.; Analysis of reinforced concrete beams strengthened in flexure with composite laminates, *Canadian Journal of Civil Engineering*, Vol.26, 1999; p.646-654

- [5] *Ebead U.A., Marzouk H.*; Tension-stiffening model for FRP-strengthened concrete two-way slabs, *Materials and Structures/Materiaux et constructions, RILEM*, Vol.38, No.276, 2005; p.193-200
- [6] *Lu X.Z., Teng J.G., Ye L.P., Jiang J.J.*; Bond-slip models for FRP sheets/plates bonded to concrete, *Engineering Structures*, Vol.27, No.6, 2005; p.920-937
- [7] *Wong R.S., Vecchio F.J.*; Towards modeling of reinforced concrete members with externally bonded fiber-reinforced polymer (FRP) composites, *ACI Structural Journal*, Vol.100, No.1, 2003; p.47-55
- [8] *Abdel Baky H.M., Ebead U.A., Neale K.W.*; Flexural and interfacial behaviour of FRP-strengthened reinforced concrete beams, *Journal of Composites for Construction (ASCE)*, Vol.11, No.6, 2007; p.629-639
- [9] *Kotynia R., Abdel Baky H.M., Neale K.W., Ebead U.A.*; Flexural strengthening of RC beams with externally bonded CFRP systems: Test results and 3D nonlinear FE analysis, *Journal of Composites for Construction (ASCE)*, Vol.12, No.2, 2008; p.190-201
- [10] *Godat A., Neale K.W., Labossière P.*; Numerical modeling of FRP shear-strengthened reinforced concrete beams, *Journal of Composites for Construction (ASCE)*, Vol.11, No.6, 2007; p.640-649
- [11] *Godat A., Qu Z., Lu X.Z., Labossière P., Ye L.P., Neale K.W.*; Size effects for reinforced concrete beams strengthened in shear with CFRP strips, *Journal of Composites for Construction (ASCE)*, Vol.14, No.3, 2010; p.260-271
- [12] *Elsayed W.E., Ebead U.A., Neale K.W.*; Interfacial behaviour and debonding failures in FRP-strengthened concrete slabs, *Journal of Composites for Construction (ASCE)*, Vol.11, No.6, 2007; p.619-628
- [13] *Elsayed W.E., Ebead U.A., Neale K.W.*; Mechanically fastened FRP-strengthened two-way concrete slabs with and without cutouts, *Journal of Composites for Construction (ASCE)*, Vol.13, No.3, 2009; p.198-207
- [14] ADINA Automatic Dynamic Incremental Nonlinear Analysis; Finite Element Software, Version 8.3, ADINA R&D Inc., Watertown, MA, 2005
- [15] ADINA Theory and Modeling Guide, Version 8.3, ADINA R&D Inc., Watertown, MA, Vol.1, Chap.3, 2005
- [16] CSA Standard CSA-A23.3-04 Design of Concrete Structures, 3rd Edition Canadian Standards Association, Toronto, ON, 2004
- [17] *Elsayed W.E., Ebead U.A., Neale K.W.*; Studies on mechanically fastened fiber-reinforced polymer strengthening systems, *ACI Structural Engineering*, Vol.106, No.1, 2009; p.49-59
- [18] *Godat A., Neale K.W., Labossière P.*; Towards modeling FRP shear-strengthened reinforced concrete beams, Proc. 8th Int. Conf. Fiber Reinforced Polymer Reinforcement for Concrete Structures, T.C. Triantafillou, Editor, Patras, Greece, 2007
- [19] *M'Bazaa I.*; Renforcement en flexion de poutres en béton armé a l'aide de lamelles en matériaux composites: Optimisation de la longueur des lamelles, M.A.Sc. Thesis, Dept. of Civil Engineering, Univ. of Sherbrooke, Sherbrooke, Canada, 1995
- [20] *Chicoine T.*; Conception et analyse d'ancrages sur les poutres renforcées en flexion à l'aide de matériaux composites, M.A.Sc. Thesis, Dept. of Civil Engineering, Univ. of Sherbrooke, Sherbrooke, Canada, 1997
- [21] *Pellegrino C., Modena C.*; Fiber reinforced polymer shear strengthening of reinforced concrete beams with transverse steel reinforcement, *Journal of Composites for Construction (ASCE)*, Vol.6, No.2, 2002; p.104-111
- [22] *Adhikary B., Mutsuyoshi H.*; Behaviour of concrete beams strengthened in shear with carbon-fibre sheets, *Journal of Composites for Construction (ASCE)*, Vol.8, No.3, 2004; p.258-264
- [23] *Longworth J., Bizindavyi L., Wight R.G., Erki A.*; Prestressed CFRP sheets for strengthening two-way slabs in flexure, *Advanced Composite Materials in Bridges and Structures*, Canadian Society for Civil Engineering, El-Badry M. and Dunaszegi L., Eds., 2004
- [24] *Brena S.F., Bramblett R.M., Wood S.L., Kreger M.E.*; Increasing flexural capacity of reinforced concrete beams using carbon fibre-reinforced polymer composites, *ACI Structural Journal*, Vol.100, No.1, 2003; p.36-46
- [25] *Harajli M.H., Soudki K.A.*; Shear strengthening of interior slab-column connections using carbon fibre-reinforced polymer sheets, *Journal of Composites for Construction (ASCE)*, Vol.7, No.2, 2003; p.145-153
- [26] *Mosallam A.S., Mosalam K.M.*; Strengthening of two-way concrete slabs with FRP composite laminates, *Construction and Building Materials*, Vol.17, 2003; p.43-54
- [27] *Godat A., Neale K.W., Labossière P.*; Numerical modelling of shear crack angles in FRP shear-strengthened reinforced concrete beams, *Australian Journal of Structural Engineering*, Vol.11, No.2, 2011; p.87-101